

Benchmarking projected generator coordinate method for nuclear Gamow–Teller transitions

R. N. Chen,^{1,2} X. Lian,³ J. M. Yao,^{1,2,*} and C. L. Bai^{3,†}

¹School of Physics and Astronomy, Sun Yat-sen University, Zhuhai 519082, P.R. China

²Guangdong Provincial Key Laboratory of Quantum Metrology and Sensing, Sun Yat-Sen University, Zhuhai 519082, P.R. China

³College of Physics, Sichuan University, Chengdu 610065, China

(Dated: January 9, 2026)

Background: The quantum-number projected generator coordinate method (PGCM) has gained increasing attention, in part due to its combination with the in-medium similarity renormalization group (IMSRG) to describe collective excitations in medium-mass deformed nuclei, as well as nuclear matrix elements (NMEs) of neutrinoless double-beta ($0\nu\beta\beta$) decay.

Purpose: Extending the PGCM to Gamow–Teller (GT) transitions and two-neutrino double- β ($2\nu\beta\beta$) decay is nontrivial, as it requires an accurate description of not only nuclear ground states but also a large number of excited states. In this work, we aim to achieve a minimal extension of the PGCM to describe GT transition strengths in even-even nuclei and to compute the NME of $2\nu\beta\beta$ decay.

Method: Within the PGCM framework, the wave functions of odd–odd nuclei are constructed as superpositions of neutron- and proton–quasiparticle configurations built on a quasiparticle vacuum state with the average particle numbers constrained to be odd neutron and odd proton. The angular momentum and particle numbers associated with the underlying mean-field states are restored through projection techniques. Using a shell-model Hamiltonian defined in the f/p shell, we assess the validity of this approach by benchmarking GT transitions in calcium and titanium isotopes, as well as the $2\nu\beta\beta$ decay of ^{48}Ca to ^{48}Ti , against exact solutions. For comparison, we also confront our results with those obtained from configuration-interaction calculations employing different particle–hole truncation schemes, both with and without IMSRG evolution.

Results: The PGCM generally reproduces GT transitions to both low-lying and giant resonance states in $^{42-48}\text{Ca}$ and $^{42-48}\text{Ti}$. Although the agreement with exact results deteriorates as the number of valence nucleons increases, the overall description remains robust. The NME of the $2\nu\beta\beta$ decay from ^{48}Ca to ^{48}Ti is calculated without invoking the closure approximation. We find that the PGCM overestimates this matrix element by about 57%, primarily due to an overestimation of the GT transition strength from ^{48}Ti to the first excited state of ^{48}Sc . Overall, the performance of the PGCM is comparable to, and in some cases exceeds, that of the CI calculation with the two-particle–two-hole truncation for the nuclei of concerned.

Conclusions: The currently implemented PGCM framework provides a reliable description of GT transitions from even–even nuclei to low-lying states of odd–odd nuclei in regions not far from closed shells. As the number of valence nucleons increases, deviations from exact results become more noticeable, reflecting the growing importance of complex many-body correlations. These discrepancies are expected to be reduced by extending the set of generator coordinates and by incorporating the IMSRG evolution, which together offer a promising route toward further enhancing the predictive power of the PGCM framework.

I. INTRODUCTION

Nuclear weak processes, including single- β and double- β decays, are a central topic of interdisciplinary research in nuclear physics, particle physics, and astrophysics. They play a central role in elucidating nuclear stability, the nucleosynthesis of elements in the universe [1–4], and in probing physics beyond the Standard Model [5–8]. In this context, accurate nuclear matrix elements (NMEs) are indispensable, as they provide the critical link between measured observables and the underlying physics [9–11]. For example, the NME governing superallowed $0^+ \rightarrow 0^+$ Fermi transitions connects the measured half-life to the V_{ud} element of the Cabibbo–Kobayashi–Maskawa (CKM) matrix [12, 13], while the NME for neutrinoless double- β ($0\nu\beta\beta$) decay relates the decay half-life to the effective neutrino mass within the standard mechanism [14]. Because NMEs cannot be accessed directly by experiment, they must be determined through nuclear-structure calculations, which require accurate wave functions for both initial and final states, together with reli-

able transition operators. Achieving such precision remains a formidable challenge, owing to the complexity of the nuclear force and the quantum many-body problem, whose exact solution rapidly becomes intractable as the number of nucleons increases.

Nuclear weak processes are typically modeled using a variety of nuclear-structure approaches that rely on different levels of approximation. A prominent example is the $0\nu\beta\beta$ decay, for which different methods predict a wide spread in the corresponding NMEs, resulting in uncertainties of a factor of 2–3 or even larger [10, 15]. Because each model is built upon distinct approximations and effective nuclear interactions, systematically reducing these discrepancies remains highly challenging. In recent years, significant progress has been achieved by combining *ab initio* nuclear methods [16] with conventional nuclear many-body solvers, enabling the calculation of NMEs of weak processes using transition operators derived from chiral effective field theory [17]. Notable examples include the valence-space in-medium similarity renormalization group (IMSRG) [18] and the in-medium generator coordinate method (IM-GCM) [19], both of which have been successfully applied to $0\nu\beta\beta$ decay in candidate nuclei [20–23].

It is worth noting that the IM-GCM is a combination of multi-reference IMSRG [19, 24] and quantum-number projected GCM (PGCM) [25]. The former is used to capture dy-

* Contact author: yaojm8@sysu.edu.cn

† Contact author: bclphy@scu.edu.cn

namic correlations associated with high-energy particle-hole excitations, while the latter is employed to include the collective (static) correlations associated with pairing and deformation. However, extending the IM-GCM to compute NMEs for single- β decay and two-neutrino double- β ($2\nu\beta\beta$) decay is considerably more challenging than for $0\nu\beta\beta$ decay. These processes require an accurate description not only of the nuclear ground states but also of a large number of excited states, all of which may contribute significantly to the decay. This difficulty is particularly pronounced for GT transitions of even-even nuclei, where many intermediate states of the corresponding odd-odd nuclei must be treated explicitly. In such systems, numerous configurations are nearly degenerate and must be incorporated into the configuration-mixing calculation, posing substantial challenges for the PGCM framework.

In this work, we generalize the PGCM framework to odd-odd nuclear systems and apply this extended framework to investigate GT transitions in even-even Ca and Ti isotopes and to evaluate the NME of the $2\nu\beta\beta$ decay of ^{48}Ca . The wave functions of the even-even nuclei are constructed as superpositions of quantum-number-projected Hartree-Fock-Bogoliubov (HFB) states with different intrinsic quadrupole deformations, whereas those of the odd-odd nuclei are approximated as superpositions of quantum-number-projected two-quasiparticle configurations built on a HFB reference state. We benchmark this framework using a shell-model Hamiltonian defined within the fp shell for which exact solutions are available. To elucidate the origin of the discrepancies between the PGCM results and the exact solutions, we further compare our calculations with configuration-interaction (CI) results that include particle-hole excitations of different truncation levels, with and without the IMSRG evolution for the interaction and GT transition operators.

It is worth noting that several related frameworks have been applied to the study of GT transitions. For example, the performance of angular-momentum projected Hartree-Fock (PHF) with projection after variation for excitation-energy spectra has been benchmarked against full CI calculations, demonstrating that quantitative agreement can already be achieved at the PHF level [26]. In addition, both variation-after-projection and GCM within the antisymmetrized molecular dynamics framework have been applied to describe GT transitions from the ground state of ^{14}N to low-lying states of ^{14}C [27]. Isospin projection has also been implemented in combination with the PGCM for nuclear β decays [28, 29]. More recently, a density functional theory-based no-core CI framework has been extended to describe GT transitions and the NME of the $2\nu\beta\beta$ decay in ^{48}Ca [30].

This paper is organized as follows. In Sec. II, we introduce the PGCM and CI frameworks based on a shell-model Hamiltonian. Section III presents and discusses the GT transition strengths of even-even Ca and Ti isotopes obtained with both methods, in comparison with exact solutions, and also reports the NME of the $2\nu\beta\beta$ decay in ^{48}Ca . Finally, Sec. IV summarizes the main conclusions and outlines future perspectives.

II. THE METHODS

A. The Hamiltonian

The employed shell-model Hamiltonian is written in the second quantization form,

$$H = H_m - \frac{1}{4} \sum_{pqrsJM} \mathcal{V}_{pqrs}^J (-1)^{J+M} [c_p^\dagger c_q^\dagger]_{JM} [\tilde{c}_r \tilde{c}_s]_{J-M}, \quad (1)$$

where the first term H_m , called an “unperturbed” term, is given by the sum of single-particle energies ε_p ,

$$H_m = \sum_p \varepsilon_p c_p^\dagger c_p, \quad (2)$$

and the second term for the two-body residual interaction. The indices p (also q, r , and s) specifies the single-particle state of quantum numbers $t_p n_p l_p j_p$, where the 3rd-component of the isospin t_p distinguishes neutron and proton states. The J -coupled two-particle creation and annihilation operators are defined as

$$[c_p^\dagger c_q^\dagger]_{JM} = \sum_{m_p, m_q} \langle j_p m_p j_q m_q | JM \rangle c_{j_p m_p}^\dagger c_{j_q m_q}^\dagger, \quad (3)$$

and

$$[\tilde{c}_r \tilde{c}_s]_{J-M} = \sum_{m_r, m_s} \langle j_r m_r j_s m_s | J - M \rangle \tilde{c}_{j_r m_r} \tilde{c}_{j_s m_s}, \quad (4)$$

where the two particles p and q (r and s) couple to total angular momentum J , and $\tilde{c}_{jm} = (-1)^{j-m} c_{j-m}$. The \mathcal{V}_{pqrs}^J is the unnormalized two-body interaction matrix element

$$\mathcal{V}_{pqrs}^J = \mathcal{N}_{pq}^{-1}(J) \mathcal{N}_{rs}^{-1}(J) \langle pq(J) | rs(J) \rangle \quad (5)$$

where the normalization factor reads $\mathcal{N}_{pq}(J) = \sqrt{1 + \delta_{pq}(-1)^J} / (1 + \delta_{pq})$, and $|rs(J)\rangle$ are antisymmetrized and normalized two-particle states. The ε_p and \mathcal{V}_{pqrs}^J are free parameters that have been fitted to nuclear low-lying states of a particular mass region [31]. In this work, we employ the GXPF1A [32] shell model Hamiltonian, which is defined within the fp shell, consisting of the $0f_{7/2}, 0f_{5/2}, 1p_{3/2}$, and $1p_{1/2}$ spherical harmonic orbitals for both protons and neutrons on top of an ^{40}Ca inert core.

B. The projected generator coordinate method

In the PGCM, the wave function of nuclear state is constructed as a superposition of symmetry-projected HFB wave functions

$$|\Psi_m^{J_i M_i N_i Z_i} \rangle = \sum_c f_c^{J_i, m} |J_i M_i N_i Z_i c\rangle \quad (6)$$

where m is a label distinguishing the states with the same spin-parity J^π . The symbol c is a collective label for (K, \mathbf{q}) . The basis states $|J_i M_i N_i Z_i c\rangle$ are constructed as follows

$$|J_i M_i N_i Z_i c\rangle = \hat{P}_{M_i K}^{J_i} \hat{P}^{N_i} \hat{P}^{Z_i} |\Phi(\mathbf{q})\rangle. \quad (7)$$

Here $\hat{P}_{M_i K_i}^{J_i}$ is the operator that projects the intrinsic wave function $|\Phi(\mathbf{q})\rangle$ onto components with well defined angular momentum J_i , and its projection along the z -axis M_i , and body-fixed 3rd axis K_i . The operators \hat{P}^{N_i} and \hat{P}^{Z_i} project the wave function onto components with well-defined neutron number N_i and proton number Z_i . The projection operators produce basis states that are not orthonormal.

The mixing weight in (6) is determined from the variational principles which leads to the Hill-Wheeler-Griffin (HWG) equation [25]

$$\sum_{c'} [\mathcal{H}_{cc'}^{J_i} - E_m^{J_i} \mathcal{N}_{cc'}^{J_i}] f_{c'}^{J_i m} = 0, \quad (8)$$

where the Hamiltonian and norm kernels \mathcal{H} and \mathcal{N} are given by the expressions

$$\mathcal{H}_{cc'}^{J_i} = \langle \Phi(\mathbf{q}) | \hat{H} \hat{P}_{KK'}^{J_i} \hat{P}^{N_i} \hat{P}^{Z_i} | \Phi(\mathbf{q}') \rangle, \quad (9)$$

$$\mathcal{N}_{cc'}^{J_i} = \langle \Phi(\mathbf{q}) | \hat{P}_{KK'}^{J_i} \hat{P}^{N_i} \hat{P}^{Z_i} | \Phi(\mathbf{q}') \rangle, \quad (10)$$

and $E_m^{J_i}$ is the energy of the m -th state with angular momentum J_i . In this work, we only consider the GT transition from the ground state of an even-even nucleus to different states of the odd-odd nucleus. In this case, the spin parity of the ground state for the initial state is $J^\pi = 0^+$, which simplifies the calculation.

The daughter nucleus is an odd-odd nucleus, whose wave function is constructed similarly, with the basis function $|J_f M_f N_f Z_f c\rangle$ constructed as follows

$$|J_f M_f N_f Z_f c\rangle = \hat{P}_{M_f K_f}^{J_f} \hat{P}^{N_f} \hat{P}^{Z_f} A_{pn}^\dagger | \Phi(\mathbf{q}) \rangle, \quad (11)$$

where the symbol c is a collective label for $c \equiv \{K, \mathbf{q}, p, n\}$. $|\Phi(\mathbf{q})\rangle$ is a quasiparticle vacuum state from the HFB calculation with the average particle numbers constrained to be odd neutron and odd proton. The A_{pn}^\dagger is a combined operator creating one quasiparticle neutron and one quasiparticle proton,

$$A_{pn}^\dagger = \beta_p^+ \beta_n^-. \quad (12)$$

For the sake of simplicity, the HFB wave function $|\Phi(\mathbf{q})\rangle$ is restricted to have axial symmetry. In this case, quasiparticle operators do not have a well-defined total angular momentum. Instead, each is labeled by Ω^π , where $\Omega_{n(p)}$ denotes the projection of the single-quasiparticle angular momentum onto the intrinsic symmetry axis, and π represents the parity of the state. The quasiparticle pair creation operator A_{pn}^\dagger obeys the K selection rule $K_{pn} = \Omega_n + \Omega_p$ and parity selection rule $\pi_n \pi_p = +1$. We focus on the final states of odd-odd nuclei with spin-parity 1^+ , which involve components with $K_{pn} = 0, \pm 1$. These components are mixed to construct the total wave function of the final state.

The norm and Hamiltonian kernels in the HWG equation (8) for the odd-odd nuclei are slightly more complicated than those for the even-even nuclei and they are given by

$$\mathcal{N}_{cc'}^{J_f} = \langle \mathbf{q} | A_{np} \hat{P}_{KK'}^{J_f} \hat{P}^{N_f} \hat{P}^{Z_f} A_{n'p'}^\dagger | \mathbf{q}' \rangle, \quad (13)$$

$$\mathcal{H}_{cc'}^{J_f} = \langle \mathbf{q} | A_{np} \hat{H} \hat{P}_{KK'}^{J_f} \hat{P}^{N_f} \hat{P}^{Z_f} A_{n'p'}^\dagger | \mathbf{q}' \rangle \quad (14)$$

If the dimension of the quasiparticle states is M_{qp} and the number of deformed configurations is denoted as N_q , there are about $M_{qp}^4 N_q^2$ kernels to be computed. To simplify the computation, we truncate the quasiparticle configurations based on the following criterial

$$E_p + E_n \leq E_{\text{cut}}. \quad (15)$$

We choose the cut-off value $E_{\text{cut}} = 48$ MeV, which turns out to be sufficient for giving a convergent solution to the excited states of the odd-odd nuclei in the energy region of interest. Besides, if not mentioned specifically, only the lowest-energy HFB state is employed for the odd-odd nuclei, i.e., $N_q = 1$.

We solve the HWG equation (8) for both even-even and odd-odd nuclei in the standard way [25], by diagonalizing the norm kernel to obtain a basis of “natural states” and then diagonalizing the Hamiltonian H in that basis. The second diagonalization can be numerically unstable, a problem we deal with by truncating the natural basis to include only states with norm eigenvalues larger than a reasonable value.

C. The configuration-interaction (CI) method with particle-hole truncation

In the CI method, the nuclear many-body wave function $|\Psi\rangle$ is expanded in a basis of particle-hole excitations built on a reference state as

$$|\Psi\rangle = D_0 |\Phi\rangle + \sum_{m,i} D_i^m |\Phi_i^m\rangle + \sum_{mn,ij} D_{ij}^{mn} |\Phi_{ij}^{mn}\rangle + \dots, \quad (16)$$

where $|\Phi\rangle$ denotes the reference state, which is a HF state. The states $|\Phi_i^m\rangle = a_m^\dagger a_i |\Phi\rangle$ represent one-particle-one-hole (1p1h) excitations, with the indices m and i labeling particle and hole single-particle orbitals, respectively. Similarly, $|\Phi_{ij}^{mn}\rangle = a_m^\dagger a_n^\dagger a_j a_i |\Phi\rangle$ correspond to two-particle-two-hole (2p2h) excitation configurations. The ellipsis indicates higher-order particle-hole excitations.

If all A -particle- A -hole configurations are included, the CI expansion in Eq. (16) yields the exact solution of the many-body problem. In practice, however, the expansion must be truncated at a finite excitation level. The CI($mpmh$) scheme, which retains configurations up to m -particle- m -hole excitations, therefore provides a controlled framework for assessing the role of many-body correlations and for elucidating the origin of discrepancies between PGCM results and exact shell-model calculations.

The many-body Hamiltonian matrix of CI exhibits a block-diagonal structure due to the symmetries of the Hamiltonian. In the M-scheme basis, two symmetries can be exploited: rotational symmetry about the z -axis and parity symmetry. The associated symmetry operators are the z -projection of angular momentum J_z and the space inversion operator Π , with corresponding eigenvalues M and π , respectively. Consequently, only the block matrices specified by fixed values of M and π need to be considered in calculations.

For the ground state of even-even nuclei with quantum numbers $J^\pi = 0^+$, the M^π subspace must be restricted to

0^+ . For excited states of odd-odd nuclei with $J^\pi = 1^+$, both $M^\pi = 0^+$ and $\pm 1^+$ subspaces must be included. We note that the particle-hole truncation scheme used in this paper does not break rotational invariance in the many-body space. As a result, the calculated energy levels for different M values remain degenerate, making it sufficient to compute the excited states only for $M^\pi = 1^+$. Moreover, we note that only the $f_{7/2}$ orbital is evolved in the reference state. Therefore, all excitation configurations within the $f_{7/2}$ orbital are equally important to the reference determinant. Consequently, we do not include particle-hole excitations for configurations among the multiplets of the $f_{7/2}$ orbital.

III. RESULTS AND DISCUSSION

A. The GT transition matrix elements

The strength for the GT transition from the ground state (0_1^+) of an even-even nucleus to the m -th excited state (1_m^+) is given by¹

$$B(\text{GT}^\mp : 0_1^+ \rightarrow 1_m^+) = \left| \langle 1_m^+ | \sigma \tau^\mp | 0_1^+ \rangle \right|^2, \quad (17)$$

where τ^- converts a neutron to a proton. For the convenience of comparison, we introduce the distribution of strength function as follows,

$$S(\text{GT}^\mp, E, \Gamma) = \sum_m B(\text{GT}^\mp : 0_1^+ \rightarrow 1_m^+) \mathcal{L}(E, E_{1_m^+}, \Gamma) \quad (18)$$

where the Lorentzian function $\mathcal{L}(E, E_{1_m^+}, \Gamma)$ is introduced to smooth the strength function

$$\mathcal{L}(E, E_{1_m^+}, \Gamma) = \frac{1}{\pi} \frac{\Gamma/2}{(\Gamma/2)^2 + (E - E_{1_m^+})^2} \quad (19)$$

and the width Γ is set as 0.5 MeV.

Figures 1 and 2 display the strength distributions of the GT-transition from $^{42-48}\text{Ca}$ to $^{42-48}\text{Sc}$, and from $^{42-48}\text{Ti}$ to $^{42-48}\text{Sc}$, respectively. It is shown that generally the PGCM is able to reproduce the results of shell-model calculations quite well for all the cases, even though the discrepancy shows up gradually with the increase of valence nucleons. A similar performance of the CI(2p2h) as that of the PGCM is observed. Quantitatively, the PGCM performs slightly better for the low-lying transitions, but slightly worse for the high-lying states. This difference is probably attributed to the fact that the low-lying states of odd-odd Sc isotopes are dominated by the collective correlations, which can be better captured in the PGCM through the mixing of different deformed configurations. In contrast, some of the important 2p2h excitation configurations are missing in the PGCM and they have a nontrivial contribution to the GT transitions to high-lying states.

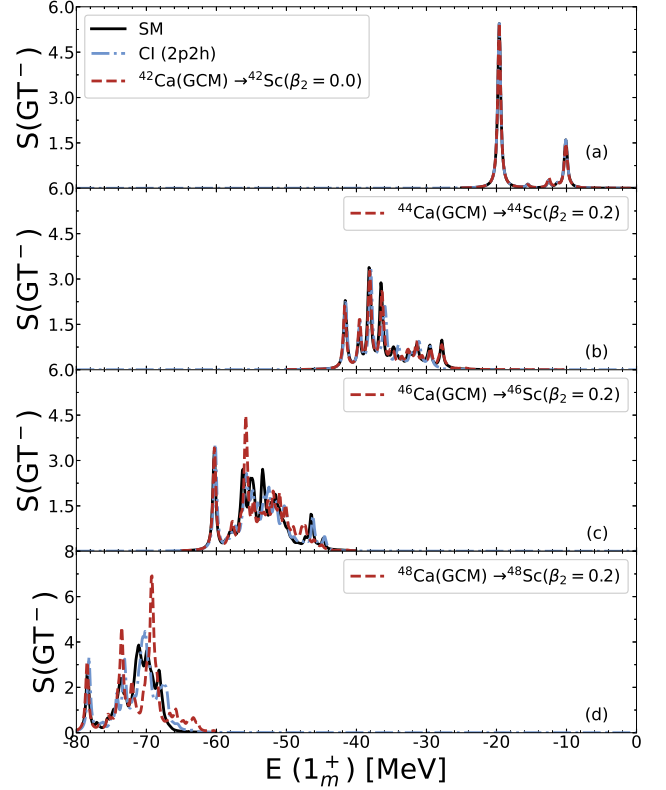


FIG. 1. (Color online) The distribution of GT^- transition strength $B(\text{GT}^- : 0_1^+ \rightarrow 1_m^+)$ from $^{42-48}\text{Ca}$ to $^{42-48}\text{Sc}$ as a function of the energy of the 1_m^+ states in $^{42-48}\text{Sc}$ isotopes from the PGCM calculation, in comparison with the results of exact shell-model and CI(2p2h) calculations.

To investigate the impact of shape mixing on the GT transition strengths, we compare in Fig. 3 the results obtained using either a purely spherical state or the GCM ground-state wave function for ^{44}Ca . The 1_m^+ states of ^{44}Sc are approximated by Eq. (11) with $\mathbf{q} \equiv \{\beta_2 = 0.2\}$. The use of the GCM wave function for ^{44}Ca considerably improves the description of the GT transition strengths to both the low-lying and high-lying 1^+ states in ^{44}Sc . Moreover, the cumulated GT strength from the exact solution is reproduced remarkably well when the GCM state is employed. These results indicate that the admixture of configurations with different shapes in the initial state leads to a substantially better agreement with the exact solution across both low- and high-energy regions.

Figure 4 shows the GT transition strengths for ^{48}Ca and ^{48}Ti obtained with GCM wave functions for the ground states of both nuclei. For the odd-odd nucleus ^{48}Sc , we restrict our analysis to cases using three different wave functions: the configuration of oblate energy minimum ($\beta_2 = -0.2$), that of the prolate energy minimum ($\beta_2 = +0.2$), and their admixture, respectively. In general, including the admixture of oblate and prolate deformed configurations improves the description of the GT transitions in both nuclei. Relative to calculations with only the prolate configuration, adding the oblate component yields a modest improvement for transitions to low-lying

¹ Note that the axial-vector coupling constant g_A is not multiplied to the GT transition operator.

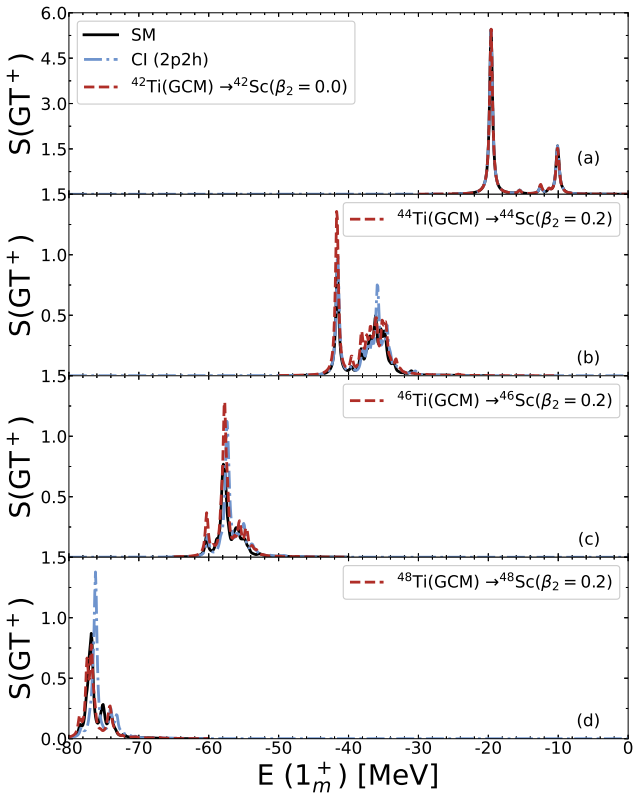


FIG. 2. (Color online) The same as Fig. 1, but for the GT⁺ transitions from $^{42-48}\text{Ti}$ to $^{42-48}\text{Sc}$, respectively.

states but leads to a substantial enhancement for transitions to high-lying states. Nevertheless, the height of the first GT peak, around $E(1_m^+) = -78.4$ MeV, for the transition from ^{48}Ti to ^{48}Sc remains significantly overestimated.

Figure 5 compares the results of the CI(1p1h) and CI(2p2h) calculations, providing insight into the impact of model-space truncation on GT transitions. For the GT⁻ transition in ^{48}Ca , extending the CI model space from 1p1h to 2p2h shifts the first peak to lower excitation energy, substantially reduces the height of the main peak, broadens its width, and brings the results into closer agreement with the exact shell-model calculation. For the GT⁺ transition in ^{48}Ti , the main peak is likewise shifted to lower energy and its height is substantially reduced, although this improvement remains insufficient to fully reproduce the exact result. Comparing the PGCM results in Fig. 4 with the CI(2p2h) results in Fig. 5, one finds that the PGCM exhibits overall better agreement with the exact shell-model result.

The in-medium similarity renormalization group (IMSRG) method [33] has achieved a remarkable success in the *ab initio* studies of atomic nuclei starting from chiral Hamiltonians. Following Ref. [19], we solve the IMSRG for ^{48}Ca starting from the shell-model interaction GXPF1A. The ground state of ^{48}Ca as a function of the flow parameter s is displayed in Fig. 6(a). It is shown that the energy converges toward the exact solution obtained by shell-model diagonalization. Using the evolved shell-model Hamiltonian, we perform CI(1p1h)

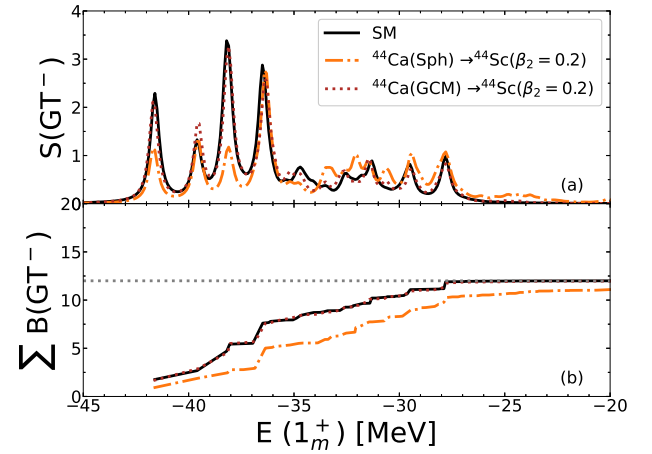


FIG. 3. (Color online) (a) The distribution of GT⁻ transition strength for ^{44}Ca as a function of the energy of the 1^+ states in ^{44}Sc . (b) The cumulated GT transition strength. The results of the PGCM calculations with the wave function of ^{44}Ca constructed using either the pure spherical state or GCM state are compared to the shell-model results.

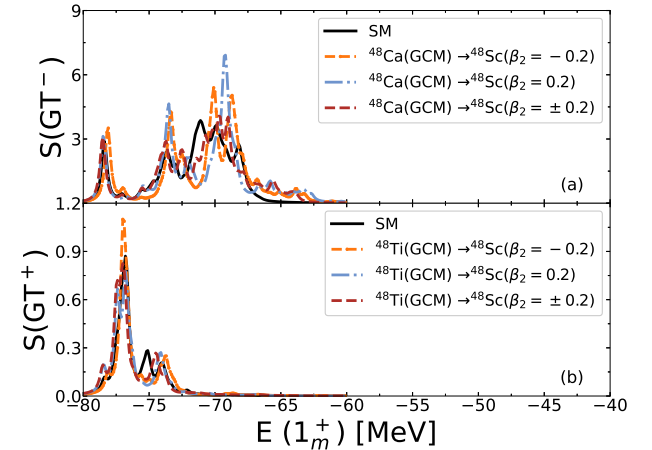


FIG. 4. (Color online) The distribution of GT transition strength for (a) ^{48}Ca and (b) ^{48}Ti as a function of the energy of the 1^+ states in ^{48}Sc from different calculations.

and CI(2p2h) calculations for the GT transition strengths from ^{48}Ca to ^{48}Sc , employing the corresponding evolved GT transition operators. For comparison, results obtained with the unevolved operators are also presented. As seen in Fig. 6(b), the IMSRG evolution leads to a modest improvement in the CI(1p1h) description; nevertheless, its performance remains slightly inferior to that of the PGCM. In contrast, the CI(2p2h) calculations with IMSRG exhibit slightly better agreement with the exact solutions than the PGCM. These observations suggest that combining the IMSRG with the PGCM could further enhance the description of GT transitions, an extension that we leave for future work.

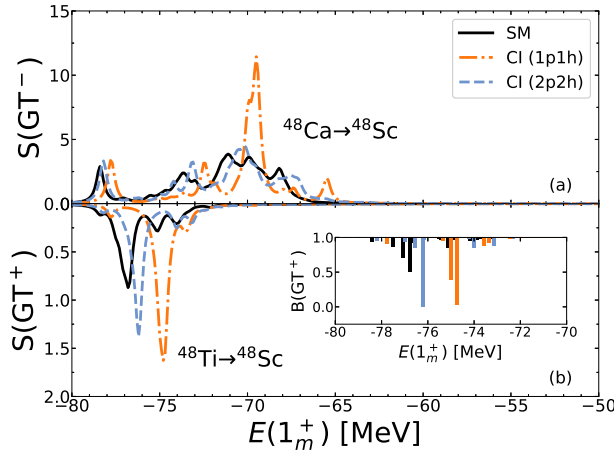


FIG. 5. (Color) The distributions of GT^- transition from ^{48}Ca (a) and GT^+ transition from ^{48}Ti as a function of the energy of the 1^+ states in ^{48}Sc , obtained from CI(1p1h), CI(2p2h) and shell-model calculations.

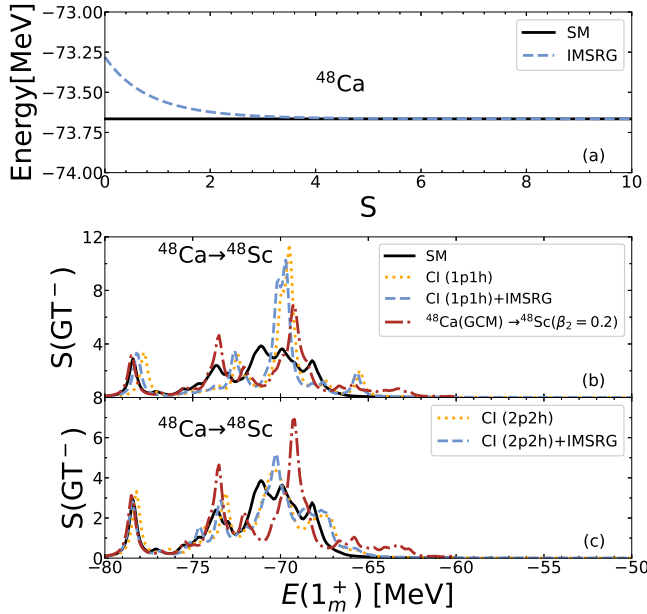


FIG. 6. (Color online) (a) The ground-state energy of ^{48}Ca as a function of the flow parameter s in the IMSRG calculation. (b) The distribution of GT^- transition strength $B(GT^- : 0_1^+ \rightarrow 1_m^+)$ from ^{48}Ca to ^{48}Sc as a function of the energy of the 1^+ states in ^{48}Sc in the CI(1p1h) calculation with or without IMSRG. (c) The same as (b) but in the CI(2p2h) calculation.

B. The NME of the $2\nu\beta\beta$ decay in ^{48}Ca

The NME of the $2\nu\beta\beta$ decay from the ground state of ^{48}Ca to that of ^{48}Ti is given by [15]

$$M^{2\nu} = \sum_m \frac{\langle 0_f^+ || \sigma\tau^- || 1_m^+ \rangle \langle 1_m^+ || \sigma\tau^- || 0_i^+ \rangle}{E(1_m^+) - [E(0_i^+) + E(0_f^+)]/2} \quad (20)$$

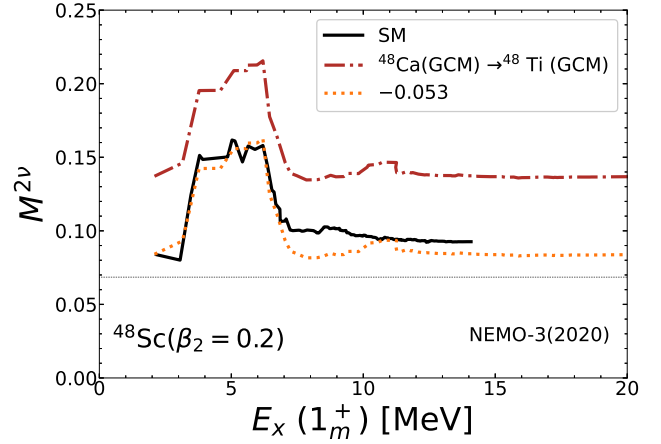


FIG. 7. (Color online) Cumulative NME $M^{2\nu}$ of $2\nu\beta\beta$ decay as a function of the excitation energy of the 1^+ states in ^{48}Sc from different calculations. The experiment data is taken from Ref.[34].

where $E(1_m^+)$, $E(0_i^+)$, and $E(0_f^+)$ are the energies of the m -th 1^+ state of the intermediate odd-odd nucleus ^{48}Sc , and the ground-state energies of ^{48}Ca and ^{48}Ti , respectively.

Using the relation

$$\begin{aligned} Q_{\beta\beta} &= E(0_i^+) - E(0_f^+) + 2(m_n - m_p - m_e) \\ &= E(0_i^+) - E(0_f^+) + 1.56 \text{ (MeV)}, \end{aligned} \quad (21)$$

one obtains

$$\begin{aligned} [E(0_i^+) + E(0_f^+)]/2 &= E(0_i^+) - [E(0_i^+) - E(0_f^+)]/2 \\ &= E(0_i^+) - (Q_{\beta\beta} - 1.56)/2 \text{ (MeV)}. \end{aligned} \quad (22)$$

The energy denominator entering the $2\nu\beta\beta$ matrix element can then be written as

$$\begin{aligned} E(1_m^+) - [E(0_i^+) + E(0_f^+)]/2 &= E(1_m^+) - E(0_i^+) + (Q_{\beta\beta} - 1.56)/2 \\ &= E_x(1_m^+) + E(6_1^+) - E(0_i^+) + (Q_{\beta\beta} - 1.56)/2 \text{ (MeV)}, \end{aligned} \quad (23)$$

where $E_x(1_m^+)$ denotes the excitation energy of the 1_m^+ state with respect to the ground state of ^{48}Sc , which has spin-parity 6_1^+ . In practice, the entire ^{48}Sc spectrum obtained from nuclear model calculations is shifted by aligning the lowest-lying 1^+ state with its experimental data. Experimentally, the energy difference between the ^{48}Sc ground state and the initial nucleus ^{48}Ca is $E(6_1^+) - E(0_i^+) = 0.503$ MeV. Substituting this value, the energy denominator becomes

$$\begin{aligned} E(1_m^+) - [E(0_i^+) + E(0_f^+)]/2 &= E_x(1_m^+) + Q_{\beta\beta}/2 - 0.277 \\ &= E_x(1_m^+) + 1.857 \text{ (MeV)}, \end{aligned} \quad (24)$$

where the experimental value $Q_{\beta\beta} = 4.2682$ MeV has been used.

Figure 7 shows the cumulated NME as a function of the excitation energy of the 1^+ states in ^{48}Sc , comparing the PGCM results with the exact shell-model calculation. The effective

NME $M_{\text{eff}}^{2\nu}$ can be derived from the half-life $T_{1/2}^{2\nu}$ based on the following formula [34],

$$T_{2\nu}^{-1} = G_{2\nu}|M_{\text{eff}}^{2\nu}|^2 = 5.3_{-0.8}^{+1.2} \times 10^{19} \text{ yr} \quad (25)$$

where $G_{2\nu} = 1.555 \times 10^{-17} \text{ yr}^{-1}$ [35] is the phase-space factor. One finds $M_{\text{eff}}^{2\nu} = 0.035 \equiv g_A^2 m_e c^2 M^{2\nu}$ [34]. If one introduces a quenching factor $q \simeq 0.78$ for the axial-vector coupling constant g_A , making $qg_A \simeq 1.0$, then one obtains the data for the $M^{2\nu}$ as follows

$$M^{2\nu} = M_{\text{eff}}^{2\nu}/(q^2 g_A^2 m_e) \simeq 0.0685 \text{ MeV}^{-1}. \quad (26)$$

This value is shown in Fig. 7 for comparison.

On the theoretical side, it is seen that most of the positive contribution to the total NME $M^{2\nu}$ of $2\nu\beta\beta$ decay comes from two of the five intermediate 1^+ states below 5 MeV excitation in ^{48}Sc and the contribution of the high-lying intermediate states is not coherent, as discussed in Ref. [36]. The final NME $M^{2\nu}$ from the exact shell-model calculation is about 0.090 MeV^{-1} [36]², about 30% larger than the data of 0.0685 MeV^{-1} .

Compared to the result by the shell-model calculation, the cumulated NME by the PGCM displays an almost constant offset of approximately -0.053 (corresponding to approximately 57% of the total value), which originates primarily from the reduced matrix element $\langle^{48}\text{Ti}(0_1^+)|\sigma\tau^-|^{48}\text{Sc}(1_1^+)\rangle$, as discussed in Fig. 4. In the PGCM calculation, the reduced matrix elements are $\langle^{48}\text{Ti}(0_1^+)|\sigma\tau^-|^{48}\text{Sc}(1_1^+)\rangle = 0.345$ and $\langle^{48}\text{Sc}(1_1^+)|\sigma\tau^-|^{48}\text{Ca}(0_1^+)\rangle = 1.568$, compared with the corresponding shell-model values of 0.241 and 1.496 , respectively. Consequently, the initial value of the $2\nu\beta\beta$ matrix-element curve is governed by the product $\langle 0_1^+|\sigma\tau^-|1_1^+\rangle \langle 1_1^+|\sigma\tau^-|0_1^+\rangle$, divided by the energy denominator, as given in Eq. (20).

IV. SUMMARY

This work presents a minimal extension of the quantum-number projected generator coordinate method (PGCM) to describe Gamow–Teller (GT) transition strengths and the nuclear matrix elements (NMEs) for the two-neutrino double-beta ($2\nu\beta\beta$) decay in even–even nuclei. By constructing states of odd–odd nuclei from quantum-number projected two quasi-particle excitations built on a HFB reference state, the approach enables a unified description of intermediate states in odd–odd nuclei within the PGCM framework. Benchmark calculations using a valence-space (fp) shell-model Hamiltonian demonstrate that the method reasonably reproduces the GT transitions to the low-lying and giant resonance states in calcium and titanium isotopes, with an overall performance comparable to, in some cases better than, configuration-interaction calculations truncated at the two-particle–two-hole level. The NME of $2\nu\beta\beta$ decay from ^{48}Ca to ^{48}Ti is also evaluated without invoking the closure approximation. The result is overestimated by approximately 57%, primarily due to the overestimated GT transition strength to the lowest-lying intermediate state. These findings establish the PGCM as a viable framework for describing β -decay observables in nuclei near closed shells and point to systematic improvements, such as extending the generator-coordinate space and incorporating the in-medium similarity renormalization group, that are expected to enhance its predictive power for more complex systems.

ACKNOWLEDGMENTS

We thank R. Wirth and H. Hergert for helpful discussions in the early stage of this work. This work was supported in part by the National Natural Science Foundation of China (Grant Nos. 12405143, 12375119, and 12141501) and the Guangdong Basic and Applied Basic Research Foundation (Grant No. 2023A1515010936).

[1] K. Langanke and G. Martínez-Pinedo, Nuclear weak-interaction processes in stars, *Rev. Mod. Phys.* **75**, 819 (2003).

[2] T. Fischer, G. Guo, K. Langanke, G. Martínez-Pinedo, Y.-Z. Qian, and M.-R. Wu, Neutrinos and nucleosynthesis of elements, *Prog. Part. Nucl. Phys.* **137**, 104107 (2024), arXiv:2308.03962 [astro-ph.HE].

[3] T. Suzuki, Nuclear weak rates and nuclear weak processes in stars, *Prog. Part. Nucl. Phys.* **126**, 103974 (2022), arXiv:2205.09262 [nucl-th].

[4] Q.-Y. Hu, L.-J. Wang, and Y. Sun, Stellar weak rates of the r -process waiting points: Effects of strong magnetic fields, *Phys. Rev. Lett.* **135**, 042702 (2025).

[5] P. Herczeg, Beta decay beyond the standard model, *Prog. Part. Nucl. Phys.* **46**, 413 (2001).

[6] N. Severijns, M. Beck, and O. Naviliat-Cuncic, Tests of the standard electroweak model in nuclear beta decay, *Rev. Mod. Phys.* **78**, 991 (2006).

[7] E. W. Otten and C. Weinheimer, Neutrino mass limit from tritium β decay, *Rep. Prog. Phys.* **71**, 086201 (2008).

[8] A. Falkowski, M. González-Alonso, and O. Naviliat-Cuncic, Comprehensive analysis of beta decays within and beyond the Standard Model, *JHEP* **04**, 126, arXiv:2010.13797 [hep-ph].

[9] F. T. Avignone, S. R. Elliott, and J. Engel, Double beta decay, majorana neutrinos, and neutrino mass, *Rev. Mod. Phys.* **80**, 481 (2008).

[10] J. Engel and J. Menéndez, Status and future of nuclear matrix elements for neutrinoless double-beta decay: a review, *Reports on Progress in Physics* **80**, 046301 (2017).

[11] H. Ejiri, Neutrino-mass sensitivity and nuclear matrix element for neutrinoless double beta decay, *Universe* **6**, 10.3390/universe6120225 (2020).

² Note that the value of $M_{\text{eff}}^{2\nu}$ does not depend on the choice of the g_A quenching factor q , while the $M^{2\nu}$ does. For example, the $M^{2\nu}$ by the shell model calculation based on Eq.(20) is $0.0539/q^2 \simeq 0.090 \text{ MeV}^{-1}$.

[12] J. C. Hardy and I. S. Towner, Superallowed $0^+ \rightarrow 0^+$ nuclear β decays: 2020 critical survey, with implications for V_{ud} and ckm unitarity, *Phys. Rev. C* **102**, 045501 (2020).

[13] N. Severijns, L. Hayen, V. De Leebeeck, S. Vanlangendonck, K. Bodek, D. Rozpedzik, and I. S. Towner, $\mathcal{F}t$ values of the mirror β transitions and the weak-magnetism-induced current in allowed nuclear β decay, *Phys. Rev. C* **107**, 015502 (2023).

[14] M. Agostini, G. Benato, J. A. Detwiler, J. Menéndez, and F. Vissani, Toward the discovery of matter creation with neutrinoless $\beta\beta$ decay, *Rev. Mod. Phys.* **95**, 025002 (2023), arXiv:2202.01787 [hep-ex].

[15] J. M. Yao, J. Meng, Y. F. Niu, and P. Ring, Beyond-mean-field approaches for nuclear neutrinoless double beta decay in the standard mechanism, *Prog. Part. Nucl. Phys.* **126**, 103965 (2022), arXiv:2111.15543 [nucl-th].

[16] H. Hergert, A Guided Tour of *ab initio* Nuclear Many-Body Theory, *Front. in Phys.* **8**, 379 (2020), arXiv:2008.05061 [nucl-th].

[17] S. Weinberg, Effective chiral Lagrangians for nucleon - pion interactions and nuclear forces, *Nucl. Phys. B* **363**, 3 (1991).

[18] S. R. Stroberg, S. K. Bogner, H. Hergert, and J. D. Holt, Nonempirical Interactions for the Nuclear Shell Model: An Update, *Ann. Rev. Nucl. Part. Sci.* **69**, 307 (2019), arXiv:1902.06154 [nucl-th].

[19] J. M. Yao, J. Engel, L. J. Wang, C. F. Jiao, and H. Hergert, Generator-coordinate reference states for spectra and $0\nu\beta\beta$ decay in the in-medium similarity renormalization group, *Phys. Rev. C* **98**, 054311 (2018), arXiv:1807.11053 [nucl-th].

[20] J. M. Yao, B. Bally, J. Engel, R. Wirth, T. R. Rodríguez, and H. Hergert, Ab initio treatment of collective correlations and the neutrinoless double beta decay of ^{48}Ca , *Phys. Rev. Lett.* **124**, 232501 (2020).

[21] A. Belley, C. G. Payne, S. R. Stroberg, T. Miyagi, and J. D. Holt, *Ab Initio* Neutrinoless Double-Beta Decay Matrix Elements for ^{48}Ca , ^{76}Ge , and ^{82}Se , *Phys. Rev. Lett.* **126**, 042502 (2021), arXiv:2008.06588 [nucl-th].

[22] A. Belley, J. M. Yao, B. Bally, J. Pitcher, J. Engel, H. Hergert, J. D. Holt, T. Miyagi, T. R. Rodríguez, A. M. Romero, S. R. Stroberg, and X. Zhang, Ab initio uncertainty quantification of neutrinoless double-beta decay in ^{76}Ge , *Phys. Rev. Lett.* **132**, 182502 (2024).

[23] A. Belley, T. Miyagi, S. R. Stroberg, and J. D. Holt, Ab initio calculations of neutrinoless $\beta\beta$ decay refine neutrino mass limits, (2023), arXiv:2307.15156 [nucl-th].

[24] H. Hergert, S. K. Bogner, T. D. Morris, S. Binder, A. Calci, J. Langhammer, and R. Roth, Ab initio multireference in-medium similarity renormalization group calculations of even calcium and nickel isotopes, *Phys. Rev. C* **90**, 041302 (2014).

[25] P. Ring and P. Schuck, *The nuclear many-body problem* (Springer-Verlag, New York, 1980).

[26] S. M. Lauber, H. C. Frye, and C. W. Johnson, Benchmarking angular-momentum projected Hartree–Fock as an approximation, *J. Phys. G* **48**, 095107 (2021), arXiv:2104.03455 [nucl-th].

[27] Y. Kanada-En’yo and T. Suhara, Gamow-Teller transitions from the ^{14}N ground state to the ^{14}C ground and excited states, *Phys. Rev. C* **89**, 044313 (2014), arXiv:1401.5517 [nucl-th].

[28] M. Konieczka, P. Bączyk, and W. Satuła, β -decay study within multireference density functional theory and beyond, *Phys. Rev. C* **93**, 042501 (2016).

[29] H. Morita and Y. Kanada-En’yo, Low-energy gamow-teller transitions in deformed $n = z$ odd-odd nuclei, *Phys. Rev. C* **98**, 034307 (2018).

[30] J. Miśkiewicz, M. Konieczka, and W. Satuła, Two-neutrino $0^+ \rightarrow 0^+$ double- β decay of ^{48}Ca within the density-functional-theory-based no-core configuration-interaction framework, *Phys. Rev. C* **112**, 055502 (2025), arXiv:2506.13747 [nucl-th].

[31] E. Caurier, G. Martinez-Pinedo, F. Nowacki, A. Poves, and A. P. Zuker, The Shell Model as Unified View of Nuclear Structure, *Rev. Mod. Phys.* **77**, 427 (2005), arXiv:nucl-th/0402046.

[32] M. Honma, T. Otsuka, B. A. Brown, and T. Mizusaki, New effective interaction for pf -shell nuclei and its implications for the stability of the $n = z = 28$ closed core, *Phys. Rev. C* **69**, 034335 (2004).

[33] H. Hergert, S. K. Bogner, T. D. Morris, A. Schwenk, and K. Tsukiyama, The In-Medium Similarity Renormalization Group: A Novel Ab Initio Method for Nuclei, *Phys. Rept.* **621**, 165 (2016), arXiv:1512.06956 [nucl-th].

[34] A. Barabash, Precise Half-Life Values for Two-Neutrino Double- β Decay: 2020 Review, *Universe* **6**, 159 (2020), arXiv:2009.14451 [nucl-ex].

[35] J. Kotila and F. Iachello, Phase-space factors for double- β decay, *Phys. Rev. C* **85**, 034316 (2012).

[36] M. Horoi, S. Stoica, and B. A. Brown, Shell-model calculations of two-neutrino double- β decay rates of ^{48}Ca with the gxf1a interaction, *Phys. Rev. C* **75**, 034303 (2007).